Scripta Materialia 164 (2019) 130–134

Contents lists available at ScienceDirect

Scripta Materialia

journal homepage: www.elsevier.com/locate/scriptamat

The effect of gradient order on mechanical behaviors of gradient nanotwinned Cu

Zhao Cheng [a,b], Lei Lu [a,*]

[a] Shengyang National Laboratory for Materials Science, Institute of Metal Research, Chinese Academy of Sciences, Shenyang 110016, China
[b] School of Materials Science and Engineering, University of Science and Technology of China, Shenyang 110016, China

ARTICLE INFO

Article history:
Received 16 January 2019
Received in revised form 29 January 2019
Accepted 2 February 2019
Available online 11 February 2019

Keywords:
Gradient nanotwinned Cu
Gradient order
Strengthening
Surface roughness
Lateral strain

ABSTRACT

Here this paper reports the gradient order effect on deformation behaviors of gradient nanotwinned (GNT) Cu samples with the same structural gradient. Tension tests indicated that the GNT Cu with normal gradient order (hard surfaces and soft core) exhibits a higher strength and a lower surface roughening during deformation than those of the GNT Cu with reverse gradient order (soft surfaces and hard core). By systematic comparison to the lateral strain and surface morphologies, it was revealed that the normal gradient order contributes to a larger strain gradient and a stronger constraint during the plastic deformation.

Gradient structures inducing strengthening and work hardening have opened an avenue towards understanding the structural gradient-related mechanical behavior [1–4]. For example, the gradient nano-grained (GNG) metals [1,2] with increasing gradually grain size from nanometer in the top surface to micrometer in the core exhibit a much enhanced yield strength, while still keeping a reasonable ductility comparing to the coarse-grained counterparts. Gradient nano-grained surface layers are responsible for the enhanced strength and able to deform plastically by grain growth in GNG Cu when the strain localization is suppressed by the gradient structure [1,5].

Most recently, gradient nanotwinned (GNT) structures [6] with dual gradient of both twin thickness and grain size that span across the entire thickness of sample were fabricated by means of direct-current electrodeposition [7]. GNT metals also exhibit an extraordinary strengthening and work hardening [6]. As the structural gradient along the gradient direction increases, both the yield strength and work hardening of GNT Cu increase simultaneously [6]. The maximum structural gradient leads to an improved yield strength that can even exceed the strongest component of the gradient microstructure [6]. The unique strengthening mechanism of GNT is attributed to ultrahigh density of geometrically necessary dislocations (GND) [8–10] forming bundles of concentrated dislocations (BCD) in grain interior, acting as strong barriers for dislocations to move and to alleviate strain localization at grain boundaries.

Among the various parameters related with the gradient structures such as the structural gradient [6], the distribution of grain size [4] and the volume fraction of nanostructure layer [11,12], the gradient order, i.e., the sequence of microstructure arrangement along the gradient direction, is also essential to the overall mechanical properties of the gradient nanostructured metals. A variety of surface manufacturing techniques for generating the gradient structures with grain size gradually increasing from the surface to the core have been investigated, including surface mechanical grinding treatment [1,11], surface mechanical attrition treatment [2], burnishing [13] and sliding deformation [14]. While reverse gradient microstructures, larger grains in the surface and finer grains in the core, were also prepared experimentally [15] and also studied in the simulation [16]. Both gradient structures with different gradient orders were believed to possess superior mechanical properties with respect to their homogeneous counterparts due to the incompatible plastic deformation along the gradient depth [2,16,17]. However, quantitative understanding the effect of gradient order on the mechanical behavior of the gradient nanostructured metals remains unclear.

In the present study, two GNT samples with quantitative identical structural gradient, but one has a normal gradient order with hard surfaces and a soft core, and another has a reverse gradient orders with soft surfaces and a hard core, are designed and fabricated by means of direct-current electrodeposition. The tensile behavior, evolution of the lateral strain and the surface morphologies of the two GNT samples during the plastic deformation are compared and the deformation mechanisms are discussed.

By means of the direct-current electrodeposition technique, four homogenous nanotwinned Cu samples (99.995 wt%) named by Ⓐ, Ⓑ, Ⓒ and Ⓓ, with increasing twin thickness and grain size, were prepared at the electrolyte temperature of 20, 25, 30 and 35 °C, respectively [7].

* Corresponding author.
E-mail address: llu@imr.ac.cn (L. Lu).

https://doi.org/10.1016/j.scriptamat.2019.02.006
1359-6462/

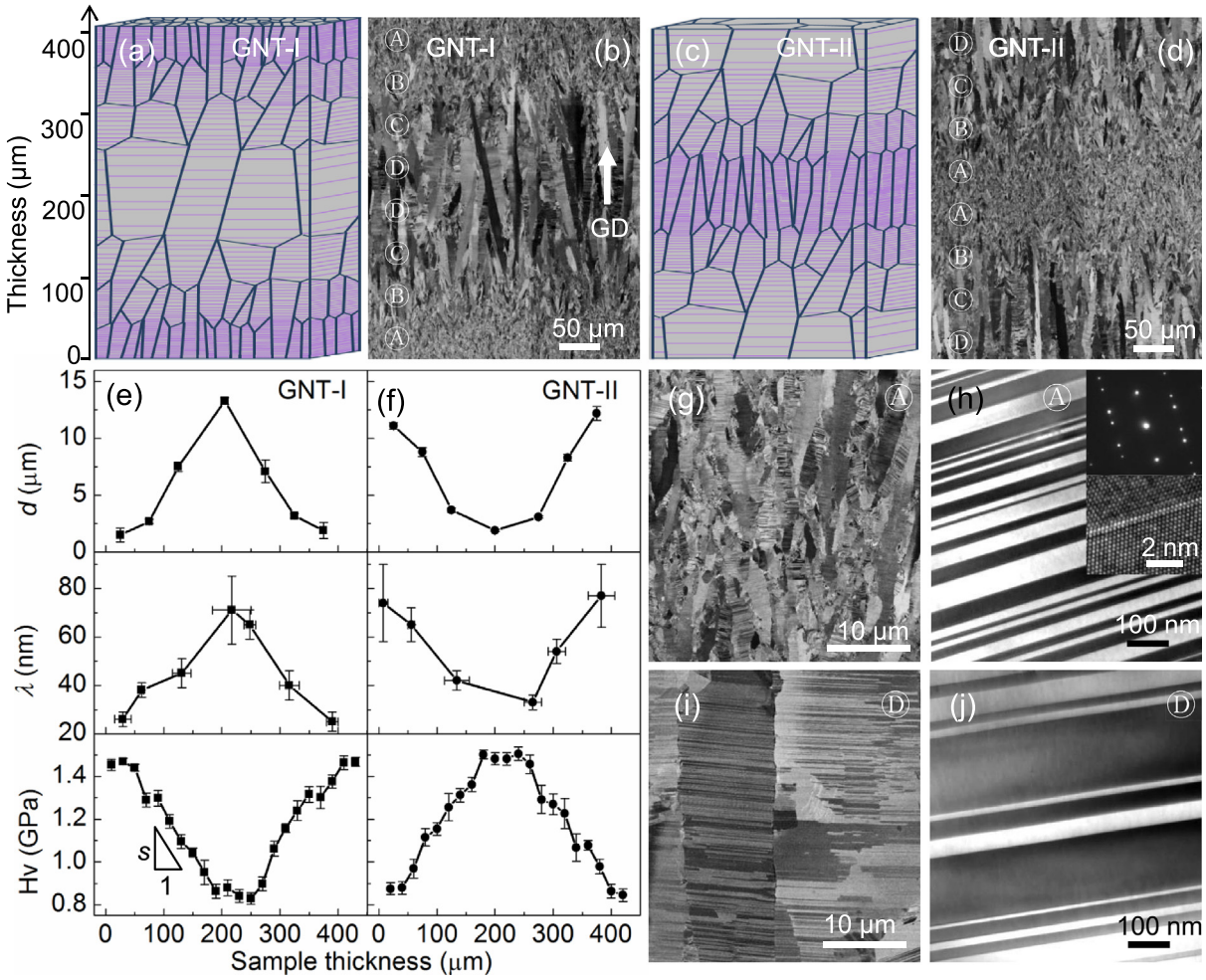

Fig. 1. The microstructure of two GNT structures with different gradient orders. The schematic (a) and the SEM image (b) of GNT-I with a gradient order of ⒶⒷⒸⒹⒹⒸⒷⒶ. The schematic (c) and the SEM image (d) of GNT-II with a gradient order of ⒹⒸⒷⒶⒶⒷⒸⒹ. The grain size, *d*, the twin thickness, λ, and the cross-sectional micro-hardness, Hv, vary with sample thickness in GNT-I (e) and GNT-II (f), respectively. The magnified SEM image (g) and the TEM image (h) of component Ⓐ in GNT-I. The SEAD pattern and the high-resolution TEM image of nanotwinned structures in the inset of (h). The SEM image (i) and TEM image (j) of component Ⓓ in GNT-I. GD, growth direction. *s*, structural gradient.

When the temperature was elevated stepwise from 20, 25, 30 to 35 °C then decreased stepwise from 35, 30, 25 to 20 °C, a GNT sample with a spatial gradient order of ⒶⒷⒸⒹⒹⒸⒷⒶ (Fig. 1(a)) was synthesized, hereafter referred to as the GNT-I. Compared to the GNT-I, the sample with a reverse spatial gradient order of ⒹⒸⒷⒶⒶⒷⒸⒹ (referred to as the GNT-II, Fig. 1(c)) was synthesized with the temperate decreasing stepwise from 35 to 20 °C firstly and then elevated from 20 to 35 °C. For both GNT-I and GNT-II samples, the deposition processes were preserved for 4 h at each temperature to make sure that each component possesses a constant volume fraction of 25%. The total deposition time for each GNT sample was kept to 16 h and then the overall sample thickness was ~400 μm.

Uniaxial quasi static tensile tests for all specimens with a width of 2 mm and a gauge length of 5 mm were performed in an Instron 5848 micro tester at a strain rate of 5×10^{-3} s^{-1} and at ambient temperature. A contactless MTS LX300 laser extensometer with displacement resolution of 1 μm was used to measure the strain during tensile tests. Cross-sectional micro-hardness of GNT samples was measured on a Qness Q10A+ micro-hardness tester with a load of 50 g and a loading time of 10 s.

The cross-sectional microstructures of GNT samples before and after tensile tests were characterized by a FEI NovaSEM 430 field emission gun scanning electron microscope (SEM) with backscattering electron imaging using a high contrast (vCD) detector and a FEI Tecnai G2 F20 transmission electron microscope (TEM) operated at 200 kV. The surface roughness and the height variation on both top and lateral surfaces of GNT samples were measured by a confocal laser scanning microscopy (CLSM, Olympus LEXT OLS4100).

The cross-sectional microstructures of the two GNT Cu samples with both normal and reverse gradient orders are characterized by SEM images in Fig. 1(b) and (d), respectively. Obviously, there are no sharp interfaces between any adjacent components along the gradient depth in both GNT samples. The magnified SEM image in Fig. 1(g) shows that component Ⓐ is composed of columnar-shaped grains with an average grain size (the size measured along the short axis) of 2 μm and a mean aspect of ~3. The magnified TEM image in Fig. 1(h) shows numerous twin lamellae with an average thickness of 26 nm are orientated preferentially perpendicular to the growth direction and embedded in these columnar grains. From the selected area electron diffraction (SAED) and the high-resolution TEM image (inserts of Fig. 1(h)), most twin planes are demonstrated to be Σ3 coherent twin boundaries (CTB). Compared to component Ⓐ, component Ⓓ has a larger grain size (13 μm) and twin thickness (71 nm), as shown in Fig. 1(i) and (j). Fig. 1(e) and (f) show the dual gradient microstructures in both GNT samples that GNT-I has increasing grain size and twin thickness but decreasing cross-sectional hardness (from 1.5 GPa to 0.8 GPa) from surfaces to the core, while the GNT-II has a reverse distribution of microstructure and hardness. The structural gradient, *s*, defined as the variation of hardness per unit sample thickness in the gradient direction which is parallel to the growth direction as indicated in Fig. 1(b), is 3.2 GPa/mm for both GNT samples as shown in Fig. 1(e) and (f).

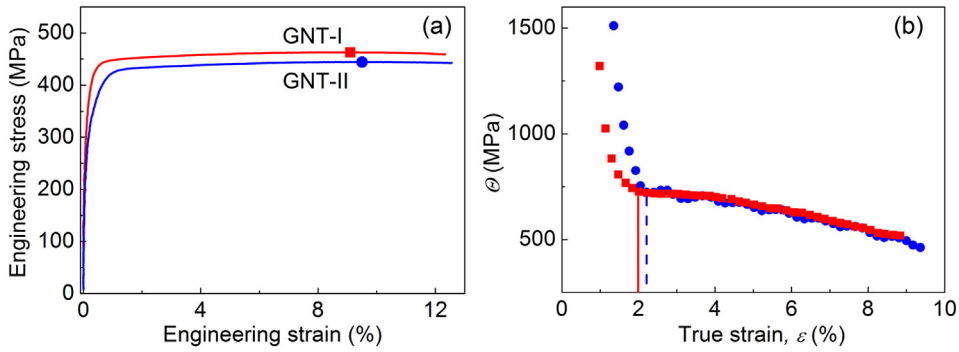

Fig. 2. Tensile engineering stress-strain curves (a) and work hardening rate, Θ, vs. true strain curves (b) of GNT-I and GNT-II samples. The inflection points, indicating where elastic-plastic transition is finished, of work hardening curves of GNT-I and GNT-II are indicated by the red solid line and the blue dash line, respectively.

The typical engineering stress-strain curves in Fig. 2(a) show that GNT-I has a higher strength and a comparable ductility with respect to that of GNT-II. From more than 6 times repeatedly tensile tests, the average yield strength and the average uniform elongation are 434 ± 12 MPa and 9.2 ± 1% for GNT-I and are 403 ± 19 MPa and 9.4 ± 0.5% for GNT-II, respectively. The corresponding work hardening rate vs. true strain curves of GNT-I and GNT-II are displayed in Fig. 2(b). For each sample, two obvious work hardening stages are detected: 1) the elastic-plastic transition stage with a steep decrease in work hardening rate before the inflection point (indicated by the solid line for GNT-I and the dash line for GNT-II) at strain of ~2%; and 2) the steady-state hardening stage with a gentle decrease at larger strains. At small strains, the inflection point of GNT-I lies at a smaller strain, i.e., the elastic-plastic transition stage of GNT-I is accomplished slightly earlier than that of GNT-II, which is consistent with the steeper tensile stress-strain curve of GNT-I in Fig. 2a. The steady-state work hardening of both GNT samples are identical, as indicated in Fig. 2b.

To demonstrate the gradient plastic deformation of GNT samples, the relative lateral strain, $\Delta\varepsilon_y$, at different sample thickness is estimated by means of the measurement of height contour on the lateral surface (the red area in Fig. 3(a)). As indicated in Fig. 3(a), the length, width and thickness direction of tension specimens are described as x, y and z axis, respectively. $\Delta\varepsilon_y$ at each sample thickness is calculated by $\Delta\varepsilon_y = 2\Delta H/W_0$, where ΔH is the height difference relative to the largest height, and W_0 is the width of the as-prepared tensile samples.

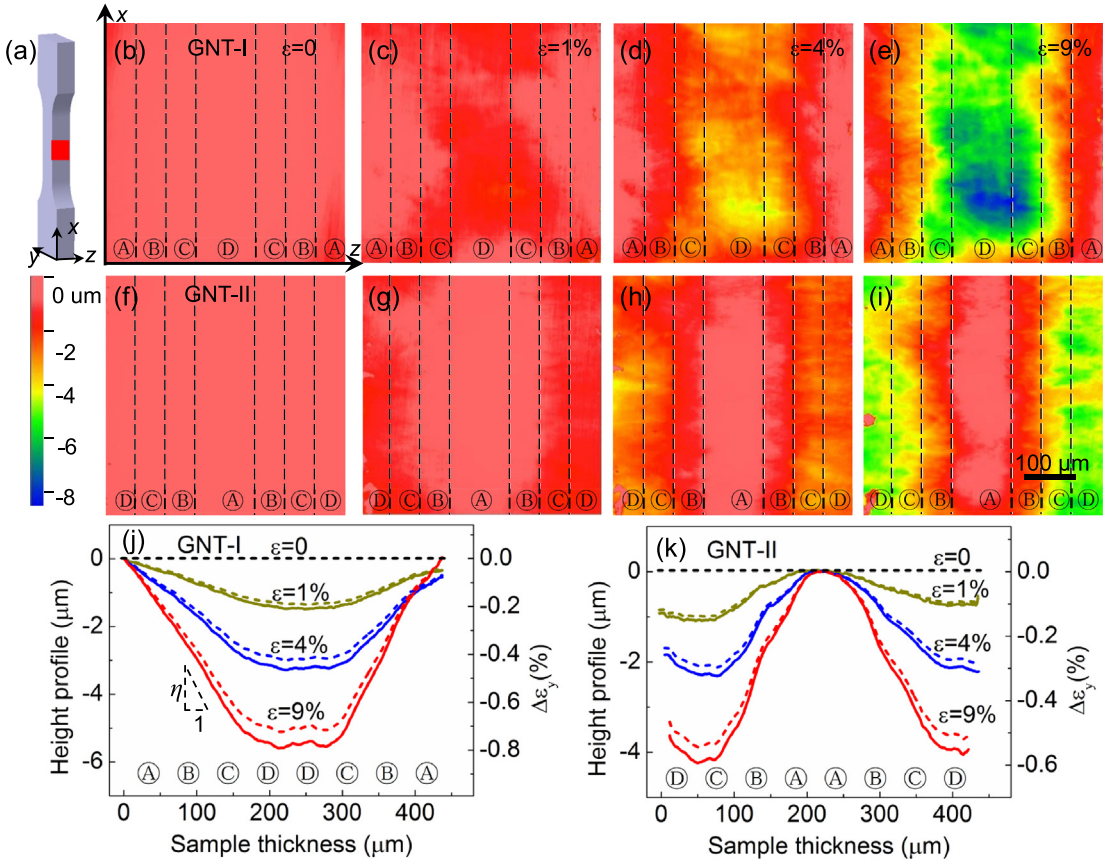

Fig. 3. Height profiles on cross-section and relative lateral strain of GNT-I and GNT-II. (a) Illustration of measurement of the height profile on lateral surface (indicated by the red area) measured by CLSM. The height contour of GNT-I (b-e) and GNT-II (f-i) deformed at $\varepsilon = 0$, 1%, 4% and 9%, respectively. Average height profiles (solid lines) and average relative lateral strain, $\Delta\varepsilon_y$, (dash lines) of GNT-I (j) and GNT-II (k) deformed at $\varepsilon = 0$, 1%, 4% and 9%, respectively. η, strain gradient.

The lateral surface of undeformed GNT-I sample is very flat as shown in Fig. 3(b). Interestingly, when GNT-I is deformed at $\varepsilon = 1\%$ the lateral surface exhibits a gradient contour that the height decreases gradually from the both surfaces to the middle (Fig. 3(c)). As the strain increases, the gradient height contour becomes more obvious as indicated in Fig. 3 (d) and (e). Such a gradient deformation is also consistent with that in a GNG Cu sample under tensile deformation under crystal plasticity finite element model [17].

To quantitatively characterize the evolution of height profile on the lateral surface with the applied strain, average height profiles (solid lines) are taken along the *x* axis in Fig. 3(j). Correspondingly, the absolute value of relative lateral strain, $|\Delta\varepsilon_y|$, increases gradually from the both surfaces to the core, as indicated by the dash lines in Fig. 3(j). The strain gradient, η, estimated by the variation of the lateral strain with sample thickness, increases from 10 m^{-1} to 35 m^{-1} when GNT-I is deformed from $\varepsilon = 1\%$ to $\varepsilon = 9\%$.

Compared to GNT-I, GNT-II exhibits a reverse deformation on the lateral surface where the height increases or $|\Delta\varepsilon_y|$ decreases gradually from the both surfaces to the middle as shown Fig. 3(f–i) and (k). The strain gradient, η, of GNT-II increases from 5 m^{-1} to 25 m^{-1} from $\varepsilon = 1\%$ to $\varepsilon = 9\%$, which is slightly lower than that of GNT-I.

To further clarify the different deformation behavior of both GNT samples, deformation morphologies of the top surface (x-y plane indicated by the insert in Fig. 4(h)) were observed by SEM and CLSM. As shown in Fig. 4(a), no obvious slip band is observed on the surface of GNT-I at $\varepsilon = 1\%$. The surface morphologies are unchanged with increasing strain as shown in Fig. 4(b) and (c). The surface height variation of GNT-I indicated by red dash lines in Fig. 4 (g) show that the original surface is very flat without any obvious fluctuation. The smooth surfaces of GNT-I keep almost constant until the applied strain is up to 9%. Correspondingly, the surface roughness of GNT-I has a negligible increment from $\varepsilon = 0$ to $\varepsilon = 4\%$ and gets clear at $\varepsilon = 9\%$ (Fig. 4(h)).

Contrary to GNT-I, typical parallel slip bands (indicated by red arrows) appear on the surface of GNT-II at $\varepsilon = 1\%$ and become more prevailing with increasing strain as displayed in Figs. 4(d-f). The noticeable fluctuation is observed at surfaces when GNT-II deformed at $\varepsilon = 1\%$ and substantially increases with increasing strain as indicated the blue solid lines in Fig. 4(g). Moreover, the surface roughness of GNT-II significantly increases with the increasing strain (Fig. 4(h)) and much larger than that of GNT-I at any strains.

Above experimental results clearly indicate that the gradient order plays a critical role in mechanical behaviors of GNT samples. Generally, the plastic deformation starts from the surface and then extends successively into the inside in the homogenous microstructures [18–22], because the microstructures at free surfaces are under less strain

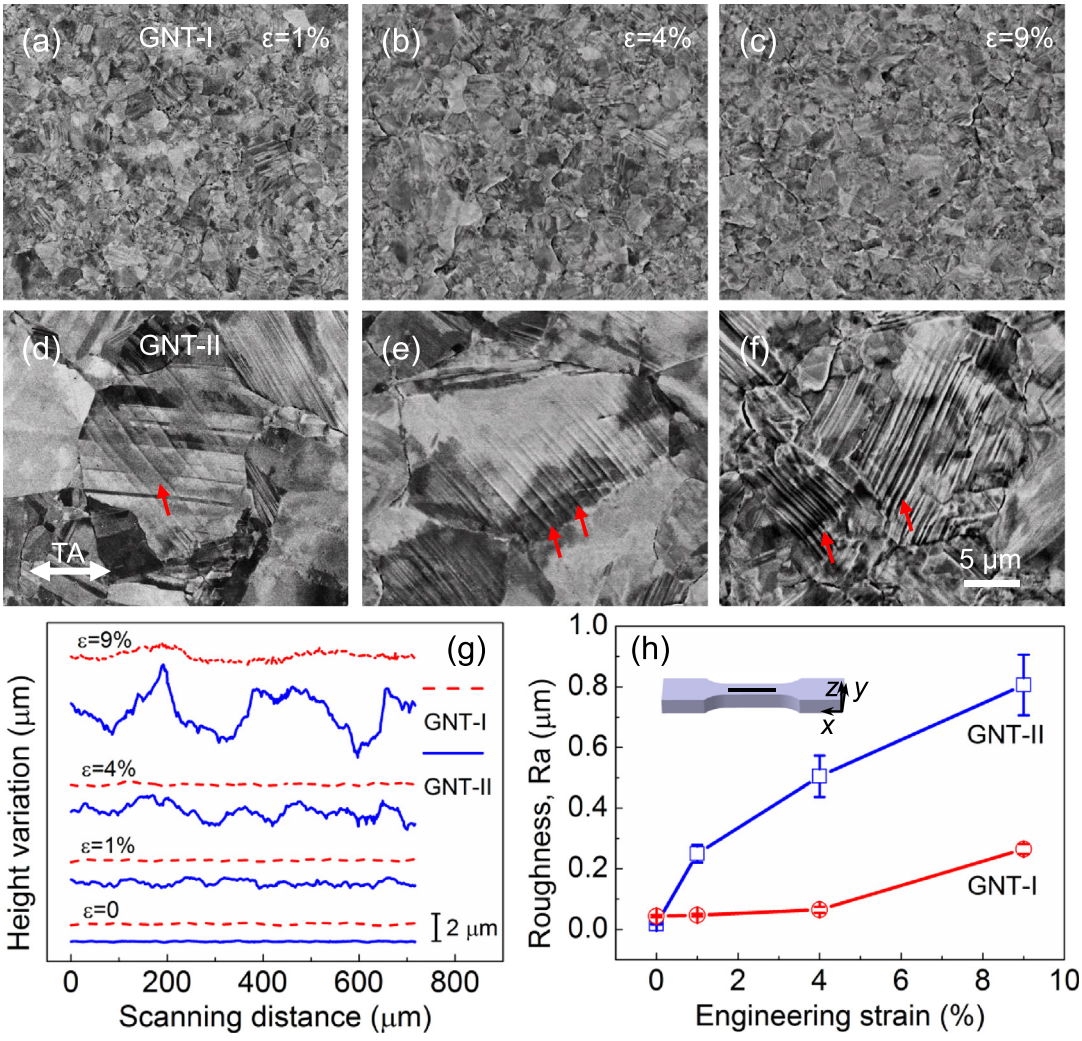

Fig. 4. Deformation morphologies on top surface of GNT-I and GNT-II. SEM images on top surface of GNT-I (a-c) and of GNT-II (d-f) at different strains as indicated. The slip bands are indicated by red arrows. (g) Measured height variation profiles on the top surface of GNT-I (dash lines) and GNT-II (solid lines) at different stains. (h) The variation of corresponding surface roughness of both GNT samples with increasing strains. The insert of (h) illustrates the measurement of height variation and roughness on top surface of GNT samples. TA, tensile axis.

constraint than that in the internal of sample, as the so-called surface effect [22].

In this study, an additional progressively plastic deformation [6,16,17] occurs in GNT samples due to the existence of dual gradient microstructure in both the grain size and twin thickness. The component Ⓓ with the largest grain size and twin thickness yields firstly under tension, and then component Ⓒ deforms plastically before component Ⓑ. Component Ⓐ with finest microstructure shall yield finally compared to the other three components.

For GNT-I with a normal gradient order of ⒶⒷⒸⒹⒹⒸⒷⒶ, the plastic deformation starts from the sample center and then progressively extends to the surfaces, which results in the decreasing $|\Delta\varepsilon_y|$ from the sample center to the surfaces (Fig. 3(j)). The surface effect inducing plastic deformation of GNT-I is effectively offset by the preferential plastic deformation occurring in the center of sample. While, for GNT-II with a reverse gradient order of ⒹⒸⒷⒶⒶⒷⒸⒹ, the plastic deformation starts from the surface and then extends into the center (Fig. 3(k)). That means the surface effect is aggravated, resulting in the less constraint inside GNT-II than GNT-I. Such a stronger constraint in GNT-I may postpone the yielding of component Ⓓ and accelerate the progressive yielding from component Ⓓ to Ⓐ, both of which lead to the faster elastic-plastic transition and the decreasing in work hardening at small strain in GNT-I, as shown in Fig. 2.

As shown in Fig. 3(j) and (k), the strain gradient of GNT-I is larger than that of GNT-II. According to the classic theory of strain gradient plasticity, geometrically necessary dislocations (GND) shall be produced to accommodate the strain gradient induced by the non-uniform deformations such as indentation, bending and torsion [8–10,23]. Consider that the density of GNDs is proportional to the strain gradient and more GNDs will produce more strengthening [8,9], the larger strain gradient of GNT-I is consistent with the mechanical properties that higher yield strength is observed in GNT-I under tension test (Fig. 2(a)).

The much smaller surface roughness of GNT-I is another advantage with respect to that of GNT-II (Fig. 4). The incompatible deformation between neighboring grains with different orientations in coarse-grained metals usually causes the deformed grains to move perpendicular to the free surface and then results in surface roughening [24]. Reducing the grain size would reduce the incompatibility of grains and the surface roughening of materials will be reduced accordingly [20,25]. For example, the surface roughness of GNG Cu with the nano-grained surface, where the strain localization or incompatible deformation is suppressed by the gradient structure [1,5], is slightly changed during tension. As expected, the surface roughening of GNT-I with fine surface microstructure is effectively decreased, as shown in Fig. 4.

Homogenous Cu with highly preferentially oriented nanoscale twins generally exhibits a strong plastic deformation anisotropy that the lateral strain along the sample width, $|\varepsilon_y|$, is much larger than the strain along the sample thickness, $|\varepsilon_z|$, during the tensile deformation [26]. Taking component Ⓓ as an example, it is clear that both height variation and surface roughness of component Ⓓ of GNT-II (at the free surfaces) are much larger (Fig. 4(g) and (h)) than those of component Ⓓ of GNT-I (in the interior). That suggests a larger plastic deformation normal to the surface [24] or a larger $|\varepsilon_z|$ occurs in the component Ⓓ of GNT-II, which is also accompanied with a lower $|\varepsilon_y|$. Accordingly, the difference of the lateral strains, $|\Delta\varepsilon_y|$, among component Ⓓ and other three components is reduced in GNT-II, as a result, a smaller lateral strain gradient will be achieved in GNT-II, compared to that of GNT-I (Fig. 3(j) and (k)).

Gradient structure with a normal gradient order (hard skin (s) covering a soft substrate) is also in favor of its fatigue [27,28] and wear resistance [29]. Fatigue crack initiation will be suppressed by the hard surface and the soft interior is effective in further arresting the crack propagation [27,28]. The highly deformable gradient nanostructured surface layer, either nano-grains in [1] or nanotwins in this study, eliminates the deformation-induced surface roughening, which suppresses surface cracking and facilitates subsequent deformation processing.

In summary, we found GNT-I with a normal gradient order of hard surfaces and soft core possesses higher strength and lower surface roughness, with respect to GNT-II with a reverse gradient order. The finer microstructure at the surfaces leads to the lower surface roughening in GNT-I during the tensile deformation. The stronger constraint and the larger strain gradient induced by a unique deformation sequence from sample center to surface contribute the improved strength for GNT-I.

Acknowledgments

L. L. acknowledges the financial support by the National Science Foundation of China (Grant Nos. 51471172, 51420105001 and U1608257) and the Key Research Program of Frontier Science, CAS. We thank Mr. S. Jin for his assistance in sample preparation.

References

[1] T.H. Fang, W.L. Li, N.R. Tao, K. Lu, Science 331 (2011) 1587–1590.
[2] X. Wu, P. Jiang, L. Chen, F. Yuan, Y.T. Zhu, Proc. Natl. Acad. Sci. U. S. A. 111 (2014) 7197–7201.
[3] Y. Wei, Y. Li, L. Zhu, Y. Liu, X. Lei, G. Wang, Y. Wu, Z. Mi, J. Liu, H. Wang, H. Gao, Nat. Commun. 5 (2014) 3580.
[4] Y. Lin, J. Pan, H.F. Zhou, H.J. Gao, Y. Li, Acta Mater. 153 (2018) 279–289.
[5] K. Lu, Science 345 (2014) 1455–1456.
[6] Z. Cheng, H. Zhou, Q. Lu, H. Gao, L. Lu, Science 362 (2018) 559.
[7] Z. Cheng, S. Jin, L. Lu, Acta Metall. Sin. 54 (2018) 428–434.
[8] M.F. Ashby, Philos. Mag. 21 (1970) 399–424.
[9] N.A. Fleck, G.M. Muller, M.F. Ashby, J.W. Hutchinson, Acta Metal. Mater. 42 (1994) 475–7487.
[10] H. Gao, Y. Huang, W.D. Nix, J.W. Hutchinson, J. Mech. Phys. Solids 47 (1999) 1239–1263.
[11] H.T. Wang, N.R. Tao, K. Lu, Scr. Mater. 68 (2013) 22–27.
[12] X.L. Wu, P. Jiang, L. Chen, J.F. Zhang, F.P. Yuan, Y.T. Zhu, Mater. Res. Lett. 2 (2014) 185–191.
[13] Z. Wang, S. Basu, T.G. Murthy, C. Saldana, J. Mater. Res. 33 (2018) 1046–1056.
[14] S.Q. Deng, A. Godfrey, W. Liu, N. Hansen, Scr. Mater. 117 (2016) 41–45.
[15] K.H. Hwang, M.R. Plichta, J.K. Lee, Mater. Sci. Eng. A 114 (1989) 61–72.
[16] Y. Wang, G. Yang, W. Wang, X. Wang, Q. Li, Y. Wei, Sci. Rep. 7 (2017) 10954.
[17] Z. Zeng, X. Li, D. Xu, L. Lu, H. Gao, T. Zhu, Extreme Mech. Lett. 8 (2016) 213–219.
[18] T. Fülöp, W.A.M. Brekelmans, M.G.D. Geers, J. Mater. Proc. Technol. 174 (2006) 233–238.
[19] Y. Zhao, Y. Guo, Q. Wei, A. Dangelewicz, C. Xu, Y. Zhu, T. Langdon, Y. Zhou, E. Lavernia, Scr. Mater. 59 (2008) 627–630.
[20] L. Yang, L. Lu, Scr. Mater. 69 (2013) 242–245.
[21] S. Miyazaki, K. Shibatat, H. Fujita, Acta Metall. 27 (1979) 855–862.
[22] T.A. Kals, R. Eckstein, J. Mater. Proc. Technol. 103 (2000) 95–101.
[23] W.D. Nix, H. Gao, J. Mech. Phys. Solids 46 (1998) 411.
[24] R. Becker, Acta Mater. 46 (1998) 1385–1401.
[25] R. Mahmudi, M. Mehdizadeh, J. Mater. Proc. Technol. 80-81 (1998) 707–712.
[26] Z.S. You, L. Lu, K. Lu, Acta Mater. 59 (2011) 6927–6937.
[27] L. Yang, N.R. Tao, K. Lu, L. Lu, Scr. Mater. 68 (2013) 801–804.
[28] T. Roland, D. Retraint, K. Lu, J. Lu, Scr. Mater. 54 (2006) 1949–1954.
[29] X. Chen, Z. Han, X.Y. Li, K. Lu, Sci. Adv. 2 (2016) 7.